Implantation of engineered human microvasculature to study human infectious diseases in mouse models

Sophia Schönherr-Hellec, Eirini Chatzopoulou, Jean-Philippe Barnier, Yoann Atlas, Sébastien Dupichaud, Thomas Guilbert, Yves Dupraz, Julie Meyer, Catherine Chaussain, Caroline Gorin, et al.

iScience

CellPress
OPEN ACCESS

Article

Implantation of engineered human microvasculature to study human infectious diseases in mouse models

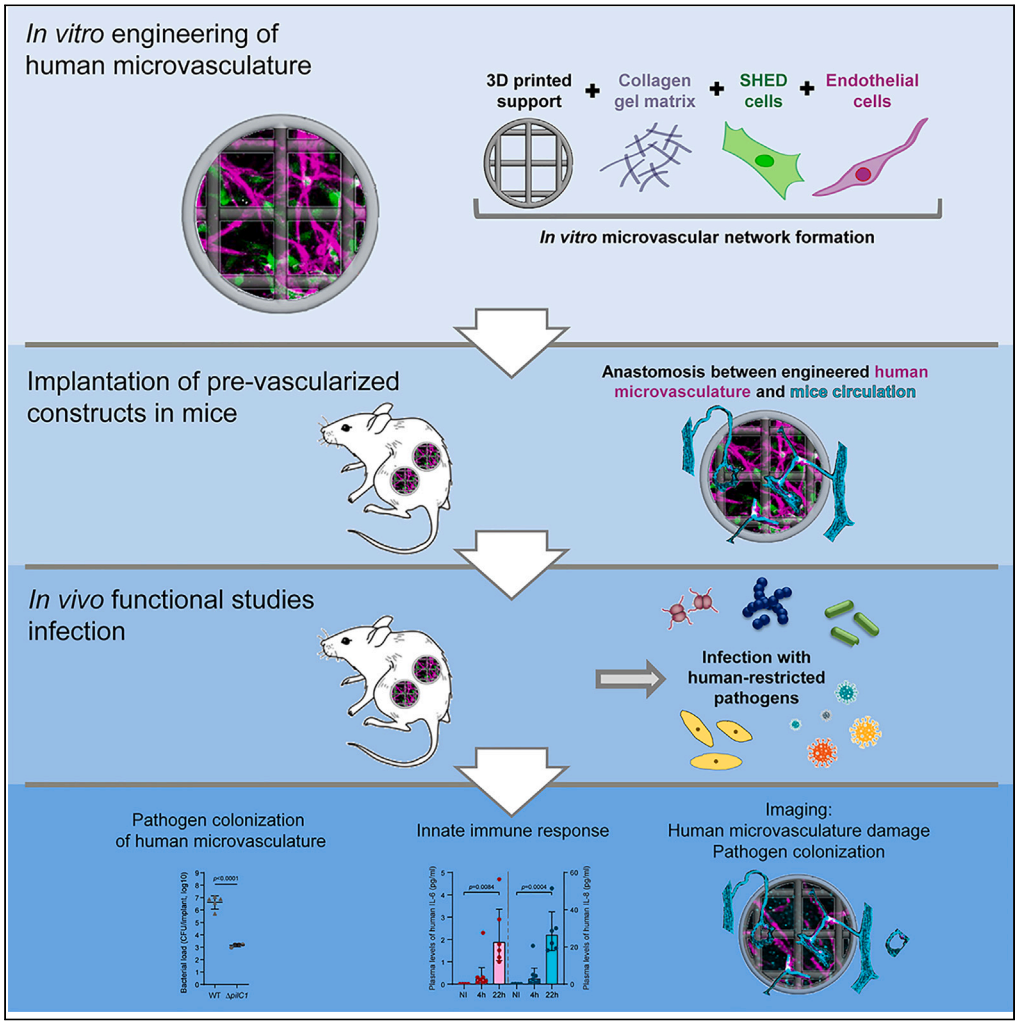

Sophia Schönherr-Hellec, Eirini Chatzopoulou, Jean-Philippe Barnier, ..., Stephane Germain, Laurent Muller, Mathieu Coureuil

laurent.muller@college-de-france.fr (L.M.)
mathieu.coureuil@inserm.fr (M.C.)

Highlights

A protocol to engineer human mature microvasculature in research lab

A blue print for 3D printed scaffold that ensures quantitative reproducibility

Imaging of implanted tissue and microvasculature

A reliable model for *in vivo* study of human infectious agents

Schönherr-Hellec et al., iScience *26*, 106286
April 21, 2023
https://doi.org/10.1016/j.isci.2023.106286

iScience

CellPress
OPEN ACCESS

Article

Implantation of engineered human microvasculature to study human infectious diseases in mouse models

Sophia Schönherr-Hellec,[1,2] Eirini Chatzopoulou,[3,9] Jean-Philippe Barnier,[1,2,9] Yoann Atlas,[4,5] Sébastien Dupichaud,[6] Thomas Guilbert,[7] Yves Dupraz,[4] Julie Meyer,[1,2] Catherine Chaussain,[3,8] Caroline Gorin,[3,8] Xavier Nassif,[1,2] Stephane Germain,[4] Laurent Muller,[4,10,*] and Mathieu Coureuil[1,2,10,11,*]

SUMMARY

Animal models for studying human pathogens are crucially lacking. We describe the implantation in mice of engineered human mature microvasculature consisting of endothelial and perivascular cells embedded in collagen hydrogel that allows investigation of pathogen interactions with the endothelium, including *in vivo* functional studies. Using *Neisseria meningitidis* as a paradigm of human-restricted infection, we demonstrated the strength and opportunities associated with the use of this approach.

INTRODUCTION

The study of human diseases and in particular human restricted infections is limited by the lack of appropriate animal models. While the transplantation of functional human cells or tissues in severe combined immunodeficient (SCID) mice has led to the generation of so-called humanized mice[1,2] that mimic some aspects of human pathologies, the development of a robust, reproducible, and reliable *in vivo* human vasculature model is still lacking.

In vivo modeling of the human vasculature is critical for the study of human pathogens that target endothelial cells to gain access to surrounding tissues and infect organs or induce vascular dysfunction associated with inflammation, ischemia, and thrombosis. Particularly important viral and bacterial human pathogens include SARS-CoV2 and *Neisseria meningitidis*, respectively. SARS-CoV2 has been shown to infect endothelial cells *in vitro* using organoid models.[3] Direct infection of endothelial cells by SARS-CoV2 has indeed been demonstrated in patients[4,5] and associated with endotheliitis and thrombosis.[6] Interestingly, in SARS-CoV2 infected patients, pre-existing vascular dysfunction was associated with a poor outcome, suggesting that endothelial cells targeted by SARS-CoV-2 are exacerbated by patients' prior condition (for review see Ionescu et al.[7]). Importantly, including SARS-CoV-2, virus-pericyte interactions have recently emerged as an important cause of endothelial dysfunction,[8] and there is currently no *in vivo* model to study human pericyte/endothelial cell interactions in the context of infection. Endothelial cells are also the target of many bacterial pathogens. *N. meningitidis* and *Streptococcus pneumoniae*, two human-restricted pathogens associated with meningitis and sepsis, interact with endothelial cells to cross the blood-brain barrier or gain access to organs where they cause significant inflammation and organ dysfunction.[9,10] *Salmonella enterica* serovar Typhi, the causative agent of typhoid fever, expresses typhoid toxin that has a particular tropism for the human-specific sialic acid present on multi-antennary glycans. Other non-exclusive human pathogens are known to interact with human endothelial cells such as *Staphylococcus aureus* or *Rickettsia* subspecies,[11,12] but the lack of *in vivo* models has hampered the understanding of the interaction between these pathogens and the endothelium.

The main strategy to study human endothelial cells *in vivo* is currently to graft human tissue, such as skin or subcutaneous fat,[13,14] in immunodeficient mice, but such models have several limitations: (1) the need to obtain human tissue, as well as the genetic and phenotypic diversity of these tissues,[15] whereas primary cells are commercially available and sold in batches that promote reproducibility of experiments; (2) the difficulty of genetically modifying human tissues, for example to mutate or invalidate host receptors or signal transducers in endothelial and/or supporting cells.

[1]Université Paris Cité, UFR de Médecine, Paris, France

[2]Institut Necker Enfants-Malades, Inserm U1151, CNRS UMR 8253, Paris, France

[3]Université Paris Cité, UPR2496 Pathologies, Imagerie et Biothérapies Orofaciales et Plateforme Imagerie du Vivant, UFR Odontologie, Paris, France

[4]Center for Interdisciplinary Research in Biology (CIRB), College de France, CNRS, INSERM, PSL Research University, Paris, France

[5]Sorbonne Université, Collège doctoral, Paris, France

[6]Cell Imaging Platform, Structure Fédérative de Recherche Necker INSERM US24/CNRS UMS3633, Paris, France

[7]Institut Cochin, INSERM U1016, CNRS UMR 8104, Université Paris Cité, Paris, France

[8]AP-HP, Services Médecines bucco-dentaire (GH Paris Sud-Sorbonne Université, Paris Nord-Université Paris Cité), Paris, France

[9]These authors contributed equally

[10]These authors contributed equally

[11]Lead contact

*Correspondence: laurent.muller@college-de-france.fr (L.M.), mathieu.coureuil@inserm.fr (M.C.)

https://doi.org/10.1016/j.isci.2023.106286

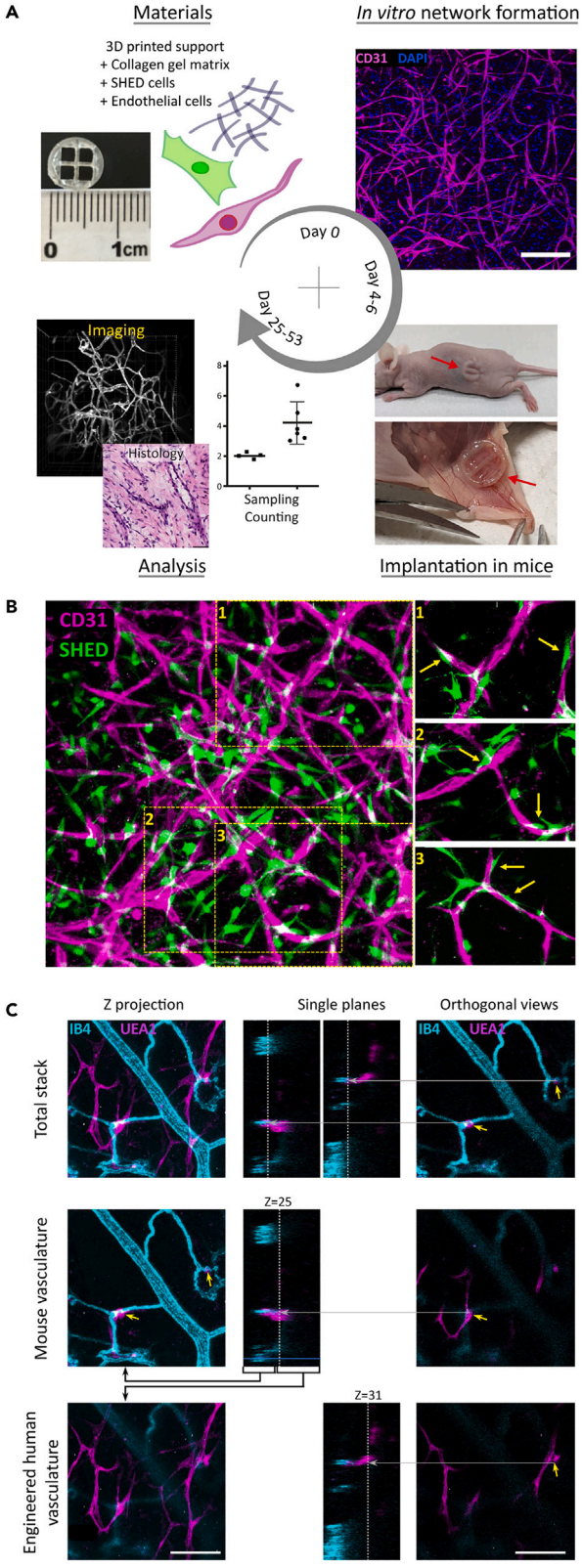
A
Materials
In vitro network formation
3D printed support
+ Collagen gel matrix
+ SHED cells
+ Endothelial cells
0
1cm
CD31 DAPI
Day 0
Day 4-6
Day 25-53
Imaging
Histology
Sampling
Counting
Analysis
Implantation in mice
B
CD31
SHED
1
2
3
C
Z projection
Single planes
Orthogonal views
IB4
UEA1
Total stack
Mouse vasculature
Z=25
Engineered human vasculature
Z=31

Figure 1. *In vitro* production of human engineered microvasculature and its anastomosis with mice vasculature after implantation

(A) Schematic representation of experimental design for implantation of engineered human microvasculature to investigate pathogen interactions with the endothelium. Human umbilical vein endothelial cells (HUVEC) and exfoliated human deciduous stem cells (SHED cells) are co-seeded in collagen gel matrix in a 3D printed scaffold (Day 0). After vascular network formation *in vitro* (Day 4), engineered microvasculature constructs are implanted subcutaneously in immunodeficient mice (Day 4–6). The human microvessels of the tissue construct anastomose with the mouse circulation thus allowing blood perfusion of the engineered human microvasculature. Three to seven weeks post-implantation mice are used for infection experiments (Day 25–53).

(B) *In vitro* network formation. After 4 days of *in vitro* co-culture of HUVECs and SHEDs expressing a GFP reporter (SHED/GFP), a microvascular network displaying perivascular recruitment has formed within the collagen gel. SHED expressed GFP (green), HUVEC were stained for CD31 (magenta). Projection of a 750 μm thick z stack. Boxed areas 1 to 3 respectively correspond to projections of 54, 144, and 51 μm-thick stacks illustrating perivascular recruitment on single capillaries with optimized fluorescence intensity. Scale bar: 100 μm.

(C) Anastomosis between engineered human microvasculature and mice circulation was detected by co-injection of *Griffonia simplicifolia* isolectin B4 specific for mouse vessels (IB4: cyan) and *Ulex europaeus* agglutinin 1 specific for human vessels (UEA-1: magenta) three weeks after implantation. Left column presents projections of total z stack (51 planes; top) or of the 22 first planes (middle: mouse vasculature) or of the 29 last planes (bottom: engineered human microvasculature). Central columns present the orthogonal views. Dotted line correspond to the z-plane indicated that is illustrated as a single plane in the right column. Yellow arrows indicate anastomosis position. Scale bar: 100 μm.

RESULTS

Engineering of a human microvasculature

To our knowledge, grafting human tissues has been applied to the study of very few pathogens colonizing either the skin (*S. aureus*) or the vessels (*N. meningitidis* and *Plasmodium falciparum*).[13,14,16,17] To circumvent these limitations, we recently developed a novel humanized mouse model based on the implantation of pre-vascularized constructs co-seeded with human umbilical vein endothelial cells (HUVECs) and mesenchymal stem cells from exfoliated human deciduous teeth (SHEDs) in SCID/Beige mice (CB17.Cg-Prkdc scid Lyst bg-J/Crl).[18] We demonstrated the improved vascular function of such implanted tissue constructs containing mature vascular networks displaying perivascular recruitment and microvascular maturation. In parallel, we demonstrated the possibility of using modified cells expressing for instance cell markers such as GFP or LifeAct-mRuby.[18]

Here, we refined the protocol for standardization and quantification of engineered human microvasculature constructs, making it accessible to a wide range of scientists (Figure 1A). We have developed a 3D-printed scaffold to support both growth of mature microvascular network *in vitro* and engraftment in immunodeficient mice (Figures 1A and S1). HUVECs and SHEDs were co-seeded in collagen upon neutralization triggering fibrillogenesis. The cell/collagen solution was transferred at once to the 3D-printed scaffold coated with poly-dopamine in order to prevent gel detachment from the scaffold as a result of contraction by cells (Figure S2).[19] Hydrogels were allowed to polymerize at room temperature before the addition of culture medium. Microvascular networks formed within 4 days by self-assembly of HUVECs promoted by VEGF and HGF released by SHEDs[20] (Figure 1B). During this period, SHEDs are recruited to capillaries through the PDGF-BB released by endothelial cells (Figure 1B), thus promoting microvascular maturation including ensheathing of both cell types within the basement membrane.[18] Tissue constructs were then implanted subcutaneously in each side of the back of immunodeficient mouse. The viability and quality of the implanted human vasculature was assessed three weeks after implantation. Lectins specific for either human (*Ulex europaeus* agglutinin 1) or mouse (*Griffonia simplicifolia* isolectin B4) vessels were co-injected in mice and analyzed by two-photon microscopy. Anastomosis between the host vasculature and human vessels was observed (Figure 1C), resulting in blood perfusion of the engrafted human microvasculature displaying human perivascular cells, as already shown using hydrogels seeded with endothelial cells only[21,22]. Taken together, these data demonstrate that grafting mature vascular network embedded in 3D printed scaffold in immunodeficient mice introduced functional human microvasculature with similar properties that we have already described.[18]

Quantification of human microvasculature infection by *N. meningitidis*

Next, we used *N. meningitidis* a human restricted pathogen to demonstrate the functionality and relevance of our model. *N. meningitidis* (the meningococcus) is a natural commensal of the human nasopharynx and a dreadful pathogen which disseminates into the bloodstream, causing cerebrospinal meningitis and severe sepsis rapidly progressing to a fatal septic shock known as *purpura fulminans*. Meningococcemia is characterized by bacterial adhesion to human endothelial cells, cytokine secretion by endothelial cells,

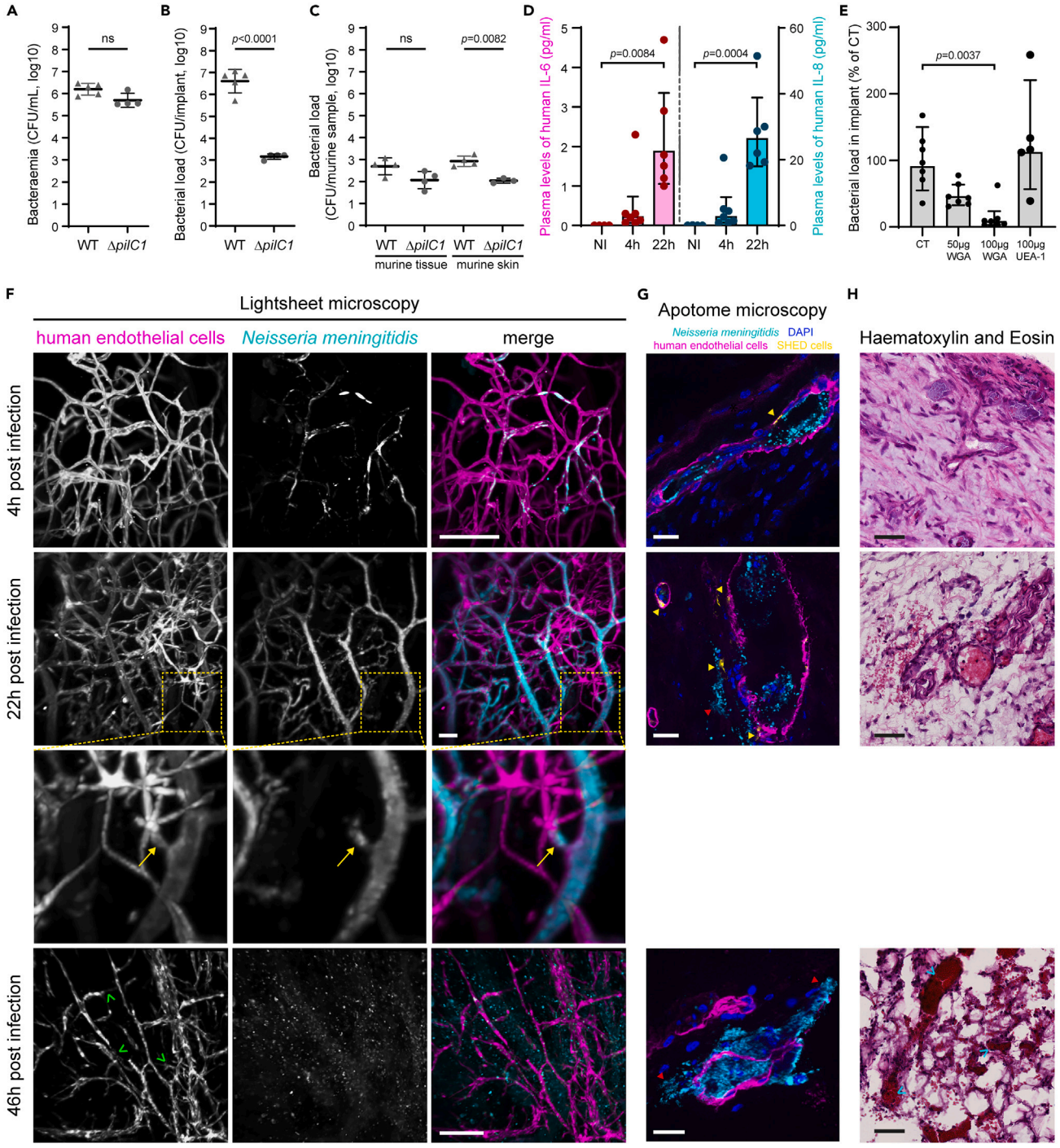

Figure 2. Characterization of meningococcal infection of the human engineered microvasculature implanted in mice

(A–C) *Neisseria meningitidis* adheres specifically to the human microvessels of the engineered construct. Mice implanted with engineered human microvasculature were infected intravenously with 3×10^6 CFU of *N. meningitidis* 2C4.3 wild type strain or its isogenic piliated non-adhesive mutant Δ*pilC1*. Bacteremia (A), implant bacterial load (B) and murine skin and subcutaneous tissue bacterial load (C) were assessed at the time of sacrifice, 3 h post-infection by quantitative culture. Bacterial counts are expressed in CFU/ml of blood and CFU/implant or CFU/murine sample.

(D) Infection with *N. meningitidis* triggers pro-inflammatory response of human endothelial cells. Human IL-6 and IL-8 concentration were measured in mouse blood before infection and 4 and 22 h post-infection. Interleukin concentrations are expressed in pg/ml of plasma.

(E) Wheat germ agglutinin (WGA) reduces bacterial load in tissue constructs. Mice implanted with engineered human microvasculature were treated with 50 or 100 µg of WGA, or with 100 µg of UEA-1 before infection with 3×10^6 CFU of *N. meningitidis* 2C4.3 wild type strain. Bacterial load was assessed at the time

Figure 2. *Continued*

of sacrifice 1 h post-infection by quantitative culture. Bacterial counts are expressed in CFU/ml of blood and CFU/implant. (A–E) Bars represent geometric mean ± geometric SD. Data were analyzed using ANOVA with Bonferroni's correction. Each dot represents one mouse. For each mouse, only one implant or skin sample were used for counting CFU.

(F–H) Mice implanted with engineered human microvasculature were infected with 3×10^6 CFU of *N. meningitidis* 2C4.3 wild type strain. After 4, 22, and 46 h of infection grafted engineered human microvasculature were removed and fixed with PFA before immunostaining with the indicated markers (F and G) or haematoxylin and eosin (H&E) stain (H). Bacteria were immunostained with anti-*N. meningitidis* (cyan) (F and G) and HUVEC were immunostained for CD31 (magenta) (F and G). Inset: obstruction is indicated with a yellow arrow (F). SHEDs expressing GFP are indicated by yellow arrowheads (yellow) (G). Extravasation of bacteria are indicated by red arrowheads (G). Nuclei were revealed with DAPI (blue) (G). At 46 h post-infection, vessels that were probably disrupted are highlighted with green arrowheads (F) and vessel obstruction is indicated with blue arrowheads (H). Scale bars: 100 (F), 20 (G), and 50 (H) μm.

vascular leakage, and thrombosis of the microvasculature.[23] Adhesion and subsequent colonization of human vessels is permitted by its type IV pili (TFP) which are adhesive filamentous protrusions made of pilin monomers.[24] Furthermore, *in vitro* experiments recently demonstrated that adhesion is promoted by TFP targeting of host cell sialylated glycans.[23,25] As a human-restricted pathogen, *N. meningitidis* adhesion is limited to cells of human origin both *in vivo* and *in vitro*.[23,25,26] These characteristics of *N. meningitidis* provide an interesting opportunity to evaluate the validity of our vascular model using mutant pathogen and to confirm *in vivo* the role of glycans in the host-pathogen interaction.

We first confirmed that *N. meningitidis* colonized the implanted engineered human microvasculature. Implanted mice were infected intravenously with 3×10^6 CFU of wild type *N. meningitidis* strain 2C4.3 and its non-adhesive derivative knockout for the *pilC1* gene (Δ*pilC1*). The latter mutant lacks adhesive TFP and is thus essential to assess the actual adhesion of meningococci to blood vessels compared to circulating bacteria. Bacteremia, implant bacterial loads and murine tissue bacterial loads were assessed at the time of sacrifice, 3 h post-infection, by quantitative culture. While bacteremia was similar between wild type and the non-adhesive Δ*pilC1* mutant, bacterial loads in implanted constructs differed significantly with an over 1000-fold decrease in bacterial load of the mutant compared to wild type (Figures 2A and 2B). Only residual bacterial load of both wild type and mutant were detected in murine skin and subcutaneous tissue (Figure 2C) as in the previous model.[27] Interestingly, a decreasing trend in bacterial load was observed for the Δ*PilC* strain. This is consistent with previous observations demonstrating that vascular colonization is necessary to maintain sustained bacteremia.[28,29] To confirm the specific adhesion of meningococci to human endothelial cells of the construct-engineered microvasculature, we compared bacteremia and bacterial load in mice implanted with 3D-printed inserts containing either a pre-vascularized collagen matrix or the matrix only (Figures S3A–S3C). Colonization of human vessels by meningococci was then followed. We observed a high bacterial load within the pre-vascularized construct for three days. On the other hand, the bacteremia of the corresponding animals began to decrease after 22 h post-infection (Figure S3D). These results demonstrate that adhesive meningococci were able to reach the engineered human microvasculature from their entry point, a lateral tail vein, via the mouse circulation and to adhere and selectively colonize the human vessels in the construct through TFP-dependent adhesion. Vascular dysfunction is commonly associated with inflammation. We therefore, demonstrated the relevance of the engineered human microvasculature construct for monitoring the secretion of human cytokines in mouse blood. We decided to follow the human cytokines IL-6 and IL-8, these pro-inflammatory cytokines are major promotors of the severity of disease in meningococcal infections that are known to be secreted by endothelial cells.[30–32] Both IL-6 and IL-8 were detected in the blood of implanted mice as early as 4 h after infection with *N. meningitidis* and reached high levels within 22 h (Figure 2D), as observed with the human skin grafted model.[29] This confirms the important role of endothelial cells in mediating inflammation during infection. We have demonstrated here that the small size of our construct is yet fully compatible with the study of inflammation and the release of specific and traceable human markers in the blood of mice.

Imaging of the engineered microvasculature construct

One major advantage of the engineered microvasculature construct is the opportunity to recover and image the microvasculature of the whole sample from sacrificed mice. To explore *N. meningitidis* colonization of the microvasculature we performed light-sheet microscopy at 4, 22, and 46 h after infection (Figure 2F, Videos S1, S2, and S3). The human vasculature revealed by species-specific anti-CD31 staining was readily visible within the implant. As early as 4 h after infection, we observed individualized microcolonies distributed in the vessels. At 22 hafter infection, bacteria have filled the human microvasculature and expanded in larger mouse vessels (Figure 2F). In some circumstances, human capillaries were devoid of pathogen downstream of what appeared to be bacterial clotting (yellow arrow in inset of Figure 2F). Independently, the

histologic analysis revealed thrombosis of vessels in the construct (Figure 2H). Furthermore, vascular leakage was detected as extravascular *N. meningitidis* staining was detected in the vicinity of human vessels (Figure 2G). At 46 h, vessels appeared to be massively damaged with dissemination of bacteria in the surrounding matrix (Figure 2G), and a trend to vascular regression (Figure 2F). We then analyzed vessels by histology and fluorescence apotome microscopy on implant cross sections (Figures 2H and S4). Altogether, hematoxylin and eosin staining revealed dramatic deterioration of the microvasculature which could be detected as early as 22 h after infection. These were associated with platelet deposition and bacteria extravasation as described previously using the skin grafted mice model.[13,27] These observations are reminiscent of the skin graft model[13,27] and also tissue biopsies in the analysis of human vessel colonization from a patient with purpura fulminans[33] or chronic meningococcaemia.[34]

Finally, we benefited from our model to confirm *in vivo* the role of sialylated containing host-glycan recognition by TFP in meningococcal adhesion. Previous results demonstrated the role of human sialic acid in the adhesion and colonization of endothelial cells by meningococci *in vitro*.[25] Here, we compared infection of mice with implanted engineered microvasculature constructs injected with physiological saline or 50 μg and 100 μg of wheat germ agglutinin (WGA), which interacts with sialic acid typically found at the terminal position of glycan chains. Fifty μg of WGA provoked a 2.6-fold reduction in implant bacterial load and 100 μg provoked an 18.1-fold reduction (Figure 2E). Conversely, we did not observe any decrease in implant bacterial load in mice injected with the control lectin Ulex europaeus agglutinin I (UEA-1), which interacts with fucose on human endothelial cells.

DISCUSSION

We have shown that our approach can be used to address a variety of questions concerning the physiology and pathology of human endothelial cells and microvasculature. Furthermore, thanks to the ease of access to the grafted material, the possibility of acquiring images of a significant portion of the grafted vascular tree, and the possibility of using modified endothelial and perivascular cells, this approach will be particularly well suited to further study vascular integrity and pathophysiology of human vascular cells infected by pathogens, including vascular damage/regression and pathogen colonization. This model will enable more precise studies of pathogen interactions with specific host factors such as human endothelial cells or pericyte receptors and could lead to major advances in the understanding and treatment of the pathogenesis of various human pathogens. Finally, great potential can be derived from this human microvasculature mouse model through the future use of genetically engineered or patient-derived human perivascular and endothelial cells.

Limitations of study

Our study does not offer a thorough examination of vessel damage or bacteria colonization using acquired images and does not include live imaging. Interactions between bacteria and perivascular cells and the fate of these cells are not addressed. Additionally, data from virus-infected mice are not included. The study only provides data using HUVEC cells, with similar results obtained using commercially available HDMEC cells, but these results are not presented in this work.

STAR★METHODS

Detailed methods are provided in the online version of this paper and include the following:

- KEY RESOURCES TABLE
- RESOURCE AVAILABILITY
  - Lead contact
  - Materials availability
  - Data and code availability
- EXPERIMENTAL MODEL AND SUBJECT DETAILS
  - Mice
  - Cell culture
- METHOD DETAILS
  - Scaffold for culture and implantation of human microvasculature
  - *In vitro* vascularization of tissue construct
  - Surgical procedure
  - *Neisseria meningitidis* strains and mouse infection
  - *Ex vivo* colony-forming units (CFU) enumeration (quantitative culture)

SUPPLEMENTAL INFORMATION

Supplemental information can be found online at https://doi.org/10.1016/j.isci.2023.106286.

ACKNOWLEDGMENTS

This work was supported by research grants ANR-19-CE14-0045-002 (to M.C.) and ANR-14-IFEC-0006-01 (to S.S. and X.N.), ANR-14-CE016-0006-01 (to C.C. and L.M.), Inserm and Université Paris Cité-IDEX (to M.C., X.N., and C.G.). Image acquisition and image analysis were performed at the Structure Fédérative de Recherche (SFR) Necker (Inserm US24/CNRS UMS3633) and at IMAG'IC core facility (Institut Cochin) which is part of the National Infrastructure France-BioImaging supported by the French research Agency (ANR-10-INBS-04). Image analysis of lighsheet acquisition were performed at the SFR Necker Image analysis platform with the help of Nicolas Goudin. EC PhD is supported by Fondation pour la Recherche Médicale. The authors want to thank Dr Christophe Helary (Laboratory of chemistry of condensed matter-LCMCP, Sorbonne-Université, Paris) for the generous gift of rat tail collagen I.

AUTHOR CONTRIBUTIONS

Conceptualization, S.S.H., L.M., and M.C.; Methodology, S.S.H., E.C., J.P.B., Y.A., L.M., and M.C.; Investigation, S.S.H., E.C., J.P.B., S.D., T.G., Y.D., J.M., L.M., and M.C.; Writing – Original Draft, S.S.H., L.M., and M.C.; Writing – Review & Editing, S.S.H., L.M., and M.C.; Funding Acquisition, X.N., S.G., L.M., and M.C.; Resources, C.C. and C.G.; Supervision, X.N., S.G., L.M., and M.C.; Project Administration, L.M. and M.C.

DECLARATION OF INTERESTS

The authors declare no competing interests.

INCLUSION AND DIVERSITY

We support inclusive, diverse, and equitable conduct of research.

Received: September 30, 2022
Revised: January 10, 2023
Accepted: February 21, 2023
Published: February 27, 2023

REFERENCES

1. Skelton, J.K., Ortega-Prieto, A.M., and Dorner, M. (2018). A Hitchhiker's guide to humanized mice: new pathways to studying viral infections. Immunology *154*, 50–61. https://doi.org/10.1111/imm.12906.

2. Stripecke, R., Münz, C., Schuringa, J.J., Bissig, K.-D., Soper, B., Meeham, T., Yao, L.-C., Di Santo, J.P., Brehm, M., Rodriguez, E., et al. (2020). Innovations, challenges, and minimal information for standardization of humanized mice. EMBO Mol. Med. *12*, e8662. https://doi.org/10.15252/emmm.201708662.

3. Monteil, V., Kwon, H., Prado, P., Hagelkrüys, A., Wimmer, R.A., Stahl, M., Leopoldi, A., Garreta, E., Hurtado Del Pozo, C., Prosper, F., et al. (2020). Inhibition of SARS-CoV-2 infections in engineered human tissues using clinical-grade soluble human ACE2. Cell *181*, 905–913.e7. https://doi.org/10.1016/j.cell.2020.04.004.

4. Godeau, D., Petit, A., Richard, I., Roquelaure, Y., and Descatha, A. (2021). Return-to-work, disabilities and occupational health in the age of COVID-19. Scand. J. Work. Environ. Health *47*, 408–409. https://doi.org/10.5271/sjweh.3960.

5. Hamming, I., Timens, W., Bulthuis, M.L.C., Lely, A.T., Navis, G.J., and van Goor, H. (2004). Tissue distribution of ACE2 protein, the functional receptor for SARS coronavirus. A first step in understanding SARS pathogenesis. J. Pathol. *203*, 631–637. https://doi.org/10.1002/path.1570.

6. Teuwen, L.-A., Geldhof, V., Pasut, A., and Carmeliet, P. (2020). COVID-19: the vasculature unleashed. Nat. Rev. Immunol. *20*, 389–391. https://doi.org/10.1038/s41577-020-0343-0.

7. Ionescu, M., Stoian, A.P., Rizzo, M., Serban, D., Nuzzo, D., Mazilu, L., Suceveanu, A.I., Dascalu, A.M., and Parepa, I.R. (2021). The role of endothelium in COVID-19. Int. J. Mol. Sci. *22*, 11920. https://doi.org/10.3390/ijms222111920.

8. Butsabong, T., Felippe, M., Campagnolo, P., and Maringer, K. (2021). The emerging role of perivascular cells (pericytes) in viral pathogenesis. J. Gen. Virol. *102*, 001634. https://doi.org/10.1099/jgv.0.001634.

9. Anil, A., and Banerjee, A. (2020). Pneumococcal encounter with the blood-brain barrier endothelium. Front. Cell. Infect. Microbiol. *10*, 590682. https://doi.org/10.3389/fcimb.2020.590682.

10. Coureuil, M., Lécuyer, H., Bourdoulous, S., and Nassif, X. (2017). A journey into the brain: insight into how bacterial pathogens cross blood-brain barriers. Nat. Rev. Microbiol. *15*, 149–159. https://doi.org/10.1038/nrmicro.2016.178.

11. Konradt, C., and Hunter, C.A. (2018). Pathogen interactions with endothelial cells and the induction of innate and adaptive immunity. Eur. J. Immunol. *48*, 1607–1620. https://doi.org/10.1002/eji.201646789.

12. Su, Z., Shelite, T.R., Qiu, Y., Chang, Q., Wakamiya, M., Bei, J., He, X., Zhou, C., Liu, Y., Nyong, E., et al. (2021). Host EPAC1 modulates rickettsial adhesion to vascular endothelial cells

via regulation of ANXA2 Y23 phosphorylation. Pathogens *10*, 1307. https://doi.org/10.3390/pathogens10101307.

13. Melican, K., Michea Veloso, P., Martin, T., Bruneval, P., and Duménil, G. (2013). Adhesion of Neisseria meningitidis to dermal vessels leads to local vascular damage and purpura in a humanized mouse model. PLoS Pathog. *9*, e1003139. https://doi.org/10.1371/journal.ppat.1003139.

14. Meehan, G.R., Scales, H.E., Osii, R., De Niz, M., Lawton, J.C., Marti, M., Garside, P., Craig, A., and Brewer, J.M. (2020). Developing a xenograft model of human vasculature in the mouse ear pinna. Sci. Rep. *10*, 2058. https://doi.org/10.1038/s41598-020-58650-y.

15. Yan, H.C., Juhasz, I., Pilewski, J., Murphy, G.F., Herlyn, M., and Albelda, S.M. (1993). Human/severe combined immunodeficient mouse chimeras. An experimental in vivo model system to study the regulation of human endothelial cell-leukocyte adhesion molecules. J. Clin. Invest. *91*, 986–996.

16. Agarwal, Y., Beatty, C., Ho, S., Thurlow, L., Das, A., Kelly, S., Castronova, I., Salunke, R., Biradar, S., Yeshi, T., et al. (2020). Development of humanized mouse and rat models with full-thickness human skin and autologous immune cells. Sci. Rep. *10*, 14598. https://doi.org/10.1038/s41598-020-71548-z.

17. Manriquez, V., Nivoit, P., Urbina, T., Echenique-Rivera, H., Melican, K., Fernandez-Gerlinger, M.-P., Flamant, P., Schmitt, T., Bruneval, P., Obino, D., and Duménil, G. (2021). Colonization of dermal arterioles by Neisseria meningitidis provides a safe haven from neutrophils. Nat. Commun. *12*, 4547. https://doi.org/10.1038/s41467-021-24797-z.

18. Atlas, Y., Gorin, C., Novais, A., Marchand, M.F., Chatzopoulou, E., Lesieur, J., Bascetin, R., Binet-Moussy, C., Sadoine, J., Lesage, M., et al. (2021). Microvascular maturation by mesenchymal stem cells in vitro improves blood perfusion in implanted tissue constructs. Biomaterials *268*, 120594. https://doi.org/10.1016/j.biomaterials.2020.120594.

19. Kim, S., Lee, H., Kim, J.A., and Park, T.H. (2022). Prevention of collagen hydrogel contraction using polydopamine-coating and alginate outer shell increases cell contractile force. Biomater. Adv. *136*, 212780. https://doi.org/10.1016/j.bioadv.2022.212780.

20. Gorin, C., Rochefort, G.Y., Bascetin, R., Ying, H., Lesieur, J., Sadoine, J., Beckouche, N., Berndt, S., Novais, A., Lesage, M., et al. (2016). Priming dental pulp stem cells with fibroblast growth factor-2 increases angiogenesis of implanted tissue-engineered constructs through hepatocyte growth factor and vascular endothelial growth factor secretion. Stem Cells Transl. Med. *5*, 392–404. https://doi.org/10.5966/sctm.2015-0166.

21. Laib, A.M., Bartol, A., Alajati, A., Korff, T., Weber, H., and Augustin, H.G. (2009). Spheroid-based human endothelial cell microvessel formation in vivo. Nat. Protoc. *4*, 1202–1215. https://doi.org/10.1038/nprot.2009.96.

22. Cheng, G., Liao, S., Kit Wong, H., Lacorre, D.A., di Tomaso, E., Au, P., Fukumura, D., Jain, R.K., and Munn, L.L. (2011). Engineered blood vessel networks connect to host vasculature via wrapping-and-tapping anastomosis. Blood *118*, 4740–4749. https://doi.org/10.1182/blood-2011-02-338426.

23. Le Guennec, L., Coureuil, M., Nassif, X., and Bourdoulous, S. (2020). Strategies used by bacterial pathogens to cross the blood-brain barrier. Cell Microbiol. *22*, e13132. https://doi.org/10.1111/cmi.13132.

24. Craig, L., Forest, K.T., and Maier, B. (2019). Type IV pili: dynamics, biophysics and functional consequences. Nat. Rev. Microbiol. *17*, 429–440. https://doi.org/10.1038/s41579-019-0195-4.

25. Virion, Z., Doly, S., Saha, K., Lambert, M., Guillonneau, F., Bied, C., Duke, R.M., Rudd, P.M., Robbe-Masselot, C., Nassif, X., et al. (2019). Sialic acid mediated mechanical activation of β2 adrenergic receptors by bacterial pili. Nat. Commun. *10*, 4752. https://doi.org/10.1038/s41467-019-12685-6.

26. Rudel, T., Scheurerpflug, I., and Meyer, T.F. (1995). Neisseria PilC protein identified as type-4 pilus tip-located adhesin. Nature *373*, 357–359.

27. Join-Lambert, O., Lecuyer, H., Miller, F., Lelievre, L., Jamet, A., Furio, L., Schmitt, A., Pelissier, P., Fraitag, S., Coureuil, M., and Nassif, X. (2013). Meningococcal interaction to microvasculature triggers the tissular lesions of purpura fulminans. J. Infect. Dis. *208*, 1590–1597. https://doi.org/10.1093/infdis/jit301.

28. Capel, E., Barnier, J.-P., Zomer, A.L., Bole-Feysot, C., Nussbaumer, T., Jamet, A., Lécuyer, H., Euphrasie, D., Virion, Z., Frapy, E., et al. (2017). Peripheral blood vessels are a niche for blood-borne meningococci. Virulence *8*, 1808–1819. https://doi.org/10.1080/21505594.2017.1391446.

29. Barnier, J.-P., Euphrasie, D., Join-Lambert, O., Audry, M., Schonherr-Hellec, S., Schmitt, T., Bourdoulous, S., Coureuil, M., Nassif, X., and El Behi, M. (2021). Type IV pilus retraction enables sustained bacteremia and plays a key role in the outcome of meningococcal sepsis in a humanized mouse model. PLoS Pathog. *17*, e1009299. https://doi.org/10.1371/journal.ppat.1009299.

30. Waage, A., Brandtzaeg, P., Halstensen, A., Kierulf, P., and Espevik, T. (1989). The complex pattern of cytokines in serum from patients with meningococcal septic shock. Association between interleukin 6, interleukin 1, and fatal outcome. J. Exp. Med. *169*, 333–338.

31. van Deuren, M., van der Ven-Jongekrijg, J., Bartelink, A.K., van Dalen, R., Sauerwein, R.W., and van der Meer, J.W. (1995). Correlation between proinflammatory cytokines and antiinflammatory mediators and the severity of disease in meningococcal infections. J. Infect. Dis. *172*, 433–439.

32. Pathan, N., Hemingway, C.A., Alizadeh, A.A., Stephens, A.C., Boldrick, J.C., Oragui, E.E., McCabe, C., Welch, S.B., Whitney, A., O'Gara, P., et al. (2004). Role of interleukin 6 in myocardial dysfunction of meningococcal septic shock. Lancet *363*, 203–209. https://doi.org/10.1016/S0140-6736(03)15326-3.

33. Pron, B., Taha, M.K., Rambaud, C., Fournet, J.C., Pattey, N., Monnet, J.P., Musilek, M., Beretti, J.L., and Nassif, X. (1997). Interaction of Neisseria maningitidis with the components of the blood-brain barrier correlates with an increased expression of PilC. J. Infect. Dis. *176*, 1285–1292. https://doi.org/10.1086/514124.

34. Dupin, N., Lecuyer, H., Carlotti, A., Poyart, C., Coureuil, M., Chanal, J., Schmitt, A., Vacher-Lavenu, M.C., Taha, M.K., Nassif, X., and Morand, P.C. (2012). Chronic meningococcemia cutaneous lesions involve meningococcal perivascular invasion through the remodeling of endothelial barriers. Clin. Infect. Dis. *54*, 1162–1165. https://doi.org/10.1093/cid/cis120.

35. Nassif, X., Lowy, J., Stenberg, P., O'Gaora, P., Ganji, A., and So, M. (1993). Antigenic variation of pilin regulates adhesion of Neisseria meningitidis to human epithelial cells. Mol. Microbiol. *8*, 719–725. https://doi.org/10.1111/j.1365-2958.1993.tb01615.x.

36. Miura, M., Gronthos, S., Zhao, M., Lu, B., Fisher, L.W., Robey, P.G., and Shi, S. (2003). SHED: stem cells from human exfoliated deciduous teeth. Proc. Natl. Acad. Sci. USA *100*, 5807–5812. https://doi.org/10.1073/pnas.0937635100.

37. Beckouche, N., Bignon, M., Lelarge, V., Mathivet, T., Pichol-Thievend, C., Berndt, S., Hardouin, J., Garand, M., Ardidie-Robouant, C., Barret, A., et al. (2015). The interaction of heparan sulfate proteoglycans with endothelial transglutaminase-2 limits VEGF165-induced angiogenesis. Sci. Signal. *8*, ra70. https://doi.org/10.1126/scisignal.aaa0963.

38. Chuah, Y.J., Koh, Y.T., Lim, K., Menon, N.V., Wu, Y., and Kang, Y. (2015). Simple surface engineering of polydimethylsiloxane with polydopamine for stabilized mesenchymal stem cell adhesion and multipotency. Sci. Rep. *5*, 18162. https://doi.org/10.1038/srep18162.

39. Park, S.E., Georgescu, A., Oh, J.M., Kwon, K.W., and Huh, D. (2019). Polydopamine-based interfacial engineering of extracellular matrix hydrogels for the construction and long-term maintenance of living three-dimensional tissues. ACS Appl. Mater. Interfaces *11*, 23919–23925. https://doi.org/10.1021/acsami.9b07912.

40. Morand, P.C., Tattevin, P., Eugene, E., Beretti, J.-L., and Nassif, X. (2001). The adhesive property of the type IV pilus-associated component PilC1 of pathogenic Neisseria is supported by the conformational structure of the N-terminal part of the molecule. Mol. Microbiol. *40*, 846–856. https://doi.org/10.1046/j.1365-2958.2001.02452.x.

STAR★METHODS

KEY RESOURCES TABLE

REAGENT or RESOURCE	SOURCE	IDENTIFIER
Antibodies and lectins		
DyLight 649-labelled Griffonia Simplicifolia isolectin B4	Vector Laboratories	#DL-1208-.5
Rhodamine-labelled Ulex Europaeus Agglutinin I	Vector Laboratories	#RL-1062-2
Wheat Germ Agglutinin	Eurobio Scientific	#L-1020-10
Ulex Europaeus Agglutinin I	Eurobio Scientific	#L-1060-5
Mouse monoclonal antibodies anti-CD31 coupled to Alexa Fluor 647	AbCam	#ab215912
Rabbit serum raised against *N. meningitidis*	Own lab	N/A
Pacific Blue (coupling kit)	Invitrogen	#P30013
Rat monoclonal antibodies anti-human-CD41	AbCam	#ab33661
Secondary antibodies raised against mouse IgG, Cy5	AbCam	#ab6563
Secondary antibodies raised against rat IgG, Cy3	AbCam	#ab98416
Secondary antibodies raised against rabbit IgG, Alexa Fluor 546	Invitrogen	# A-11035; AB_2534093
4′,6-diamidino-2- phenylindole	Invitrogen	#D1306
Enzymes, chemicals and antibiotics		
Collagenase	Worthington Biochem	#9001-12-1
Dispase® II (Roche)	Sigma-Aldrich	#4942078001
0.25% trypsin EDTA solution	Sigma-Aldrich	#59428C
Human Holo-Transferrin Protein, CF	R&D BioTechne	#2914-HT-001G
Bovine Serum Albumin	Sigma-Aldrich	#A2153
Rat tail type I collagen for engineered human construct	generous gift from Dr Christophe Helary	N/A
Rat tail type I collagen for propagation of HUVECs	Becton Dickinson	#11563550
Dental LT Clear Resin	Formlabs	#RS-F2-DLCL-02
Polydopamine	Merck	H8502
RapiClear 1.52	SunJin Lab	#RC152001
RapiClear 1.47	SunJin Lab	#RC147001
Paraformaldehyde 16% solution	Invitrogen	#28908
Triton-X-100	Sigma-Aldrich	#93443
Penicillin/streptomycin	Invitrogen	#15140122
Sodium-azide	Sigma-Aldrich	#S2002
Kanamycin monosulfate	Sigma-Aldrich	#BP861
OCT	Tissuetek	#4583
Experimental models: Bacterial strains and media		
N. meningitidis 8013 strain clone 2C4.3	(Nassif et al., 1993)[35]	N/A
N. meningitidis Δ*pilC1* derivative of 2C4.3	(Morrand et al., 2001)	N/A
RPMI-1640 medium	Invitrogen	#11875093

(*Continued on next page*)

Continued

REAGENT or RESOURCE	SOURCE	IDENTIFIER
Experimental models: Cells and media		
SHEDs	Obtained as in Miura et al., 2003[36]	N/A
Human endothelial cells from the umbilical vein	Obtained as in Beckouche et al., 2003[37]	N/A
Endothelial cell growth medium 2, ECGM2	Promocell	#C-22111
Dulbecco's Modified Eagle Medium 1 g/l D-Glucose	Invitrogen	#11885084
Fetal bovine serum	Invitrogen	#A5256701
Experimental models: Organisms/strains		
SCID/Beige (CB17.Cg-Prkdc scid Lyst bg-J /Crl)	Janvier Labs	#SM-CB17-F
Software and algorithms		
Prism 8	GraphPad	https://www.graphpad.com/scientific-software/prism
Imaris V9.5	Oxford Instruments	https://imaris.oxinst.com/versions/9-5
Illustrator	Adobe	https://www.adobe.com/fr/products/illustrator.htm

RESOURCE AVAILABILITY

Lead contact

Further information and requests for resources and reagents should be directed to the lead contact, Dr. Mathieu Coureuil (mathieu.coureuil@inserm.fr).

Materials availability

This study did not generate any new unique reagents.

Data and code availability

Data reported in this paper will be shared by the lead contact upon request. This paper does not report original code. Any additional information required to reanalyze the data reported in this paper is available from the lead contact upon request.

EXPERIMENTAL MODEL AND SUBJECT DETAILS

Mice

The animal experimental procedures described in this work conform to the European ethical regulations (Directive 2010/63/EU). The project was approved by Comité d'Ethique en matière d'Expérimentation Animale Paris Descartes and the Ministère de l'Eduction Nationale de l'Enseignement Supérieur et de la Recherche (Project Number APAFIS #29971 and #26076).

SCID/Beige (CB17.Cg-Prkdc scid Lyst bg-J /Crl) mice, purchased from Charles Rivers (France), were used in all infection experiments performed in this study. Athymic Nude Mice from Janvier (France) were used in all noninfectious experiments performed in this study. Mice were kept under standard conditions (light 07.00-19.00h; temperature 22 ± 1 °C; humidity 50 ± 10%) and received sterilized rodent feed and water *ad libitum*. For all experiments, female mice between 6 and 10-weeks of age were used.

Cell culture

SHED were prepared as previously reported.[18,36] Deciduous teeth were collected after exfoliation from healthy young children (3-7 years of age). All teeth were collected with informed and oral consent from the patients and the parents according to ethical guidelines set by the French law and with a dedicated authorization for UPR2496 (n°DC-2009-927, Cellule Bioéthique DGRI/A5, Paris, France). Briefly, teeth were decontaminated with povidone-iodine solution (Betadine) before sectioning for exposure and collection of pulp tissues. SHED were isolated by enzymatic digestion with type I collagenase (3 mg/ml) and

dispase (2 U/ml). Single-cell suspensions were then cultured in Modified Eagle Medium alpha (MEM alpha; Invitrogen) supplemented with 20% fetal bovine serum (FBS; Invitrogen), 1% penicillin/streptomycin, at 37°C with 5% CO2. Subconfluent cells were detached by trypsinization (0.25% trypsin EDTA solution), aliquoted and frozen. Experiments were performed with cells thawed at a density of 10^4 cells/cm^2 in Dulbecco's Modified Eagle Medium 1 g/l D-Glucose (DMEM low glucose; Invitrogen) supplemented with 10% FBS and 1% penicillin/streptomycin, at 37°C with 5% CO2 with medium refreshing twice a week. For all experiments, SHED were used between passages 2 and 5. Human endothelial cells from the umbilical vein (HUVECs) were prepared as previously described.[37] Human umbilical cords were provided by AP-HP, Hôpital Saint-Louis, Unité de Thérapie Cellulaire, CRB-Banque de Sang de Cordon (authorization number AC-2016-2759). They were cultivated on type I collagen (100 μg/mL) in endothelial cell growth medium 2 (ECGM2, PromoCell) refreshed every other day. Experiments were performed before passage 6. For some experiments SHEDs were transduced with a lentivirus encoding GFP as previously described.[18]

METHOD DETAILS

Scaffold for culture and implantation of human microvasculature

Scaffolds for the engineered human microvasculature were designed using Inventor (Autodesk, San Rafael, CA) and printed with Form 2 3D printer (Formlabs) using Dental LT Clear Resin. Scaffolds have a circular form of 8 mm diameter and 1.6 mm thickness crossed by 2 layers of 3 bars each of 500 μm width thus creating 4 areas of 5 mm^2 (Figure S1A). These dimensions allowed for optimal capillary formation without gel contraction. Scaffolds were printed vertically with bars at 45° in order to prevent bending (Figure S1B). Prior to casting hydrogels, scaffolds were coated overnight protected from light with 1.5 mg/ml polydopamine in order to prevent gel contraction by cells during the culture period, as previously described.[18,38,39] Briefly, polydopamine was solubilized in 2% of the final volume of H_2O before dilution in 10 mM Tris pH 8.5.

In vitro vascularization of tissue construct

Scaffolds (one scaffold per well) were placed in 48-well plates for suspension cell culture (Cellstar, Greiner bio-one). Endothelial cells ($1.5x10^6$/ml) were co-seeded with SHED ($1x10^6$/ml) in 2 mg/ml collagen I extracted from rat tail (generous gift from Dr Christophe Helary). Hydrogels were prepared on ice by mixing collagen I in 20 mM acetic acid with M199 (Invitrogen) medium and 25 mM $NaHCO_3$. Cell pellets were resuspended in serum-free medium and diluted in the collagen solution just before casting the gels in the 3D scaffold. After 40 minutes at room temperature for collagen fibrillogenesis, medium was added and hydrogels were cultured for 4 days in ECGM2 depleted for VEGF, heparine and hydrocortisone.

Surgical procedure

Tissue constructs were implanted in 6-10 weeks old SCID or athymic nude mice. Analgesia injection with buprenorphine (0.1 mg.kg-1) was performed 15 min before surgery to prevent pain. Mice were anesthetized with 80-100 mg.kg-1 of ketamine (Imalgene 1000, Boehringer, Ingelheim) and 8.5-10 mg.kg-1 of xylazine (Rompun, 2%, Bayer). Two tissue constructs were implanted subcutaneously in each side of the mouse back (Figure 1A). Wound closure was achieved using 7 mm clips (World precision instruments, USA) or 4.0 resorbable sutures (Ethicon). Grafted mice were used for experimentation 3-7 weeks post-surgery when the human microvessels of the implants were anastomosed to the mouse circulation without evidence of local inflammation. All efforts were made to minimize suffering. The day of sacrifice both implants are removed. When required, either one implant was used for counting CFU and the other was processed for imaging or both were processed for imaging.

Neisseria meningitidis strains and mouse infection

N. meningitidis 8013 strain clone 2C4.3 is a piliated, adherent and encapsulated serogroup C clinical isolate that produces the class I SB pilin variant, Opa-, Opc-, PilC1+/PilC2+, as described previously.[35] *N. meningitidis* Δ*pilC1* mutant has been previously described.[40] Strains were streaked from -80°C freezer stock onto GCB agar plates and grown overnight in a moist atmosphere containing 5% CO2 at 37°C. When needed Kanamycin (100μg/ml) was added to the plate. For all experiments, bacteria were transferred to liquid cultures in pre-warmed RPMI-1640 medium (Invitrogen) supplemented with 10% FBS at adjusted OD 600nm = 0.05, and incubated with gentle agitation for 2 hours at 37°C in the presence of 5% CO2. Bacteria were washed twice in physiological saline and resuspended to $3x10^7$ CFU.ml^{-1} in physiological saline. Prior to infection, mice were injected intraperitoneally with 8 mg of human transferrin to promote bacterial growth *in vivo*.[27] Mice were infected by intravenous injection of 100 μl of the bacterial inoculum ($3x10^6$ CFU

total). Inoculum were then determined by quantitative culture and confirmed to be between 2 to $6x10^6$ CFU total.

When needed, 50 μg or 100 μg of WGA, or 100 μg of UEA-1 resuspended in physiological saline were injected intravenously prior to infection.

Ex vivo colony-forming units (CFU) enumeration (quantitative culture)

To assess bacteremia (blood circulating bacteria) in infected animals, 10 μl of blood was sampled at 1 h, 3 h, 4 h, 22 h, 46 h after infection depending on the experiment and at the time of sacrifice. Serial dilutions of blood were plated on GCB agar plates and incubated overnight at 37°C and in a moist atmosphere containing 5% CO2. Bacterial counts were expressed as colony-forming units (CFU) per ml of blood. To assess the extent of vascular colonization by meningococci (adherent bacteria) following mouse sacrifice at indicated times post-infection, engineered human constructs (implants) or murine skin or the subcutaneous tissue below the implants were collected and placed in 500 μl of Phosphate Buffered Saline (PBS, Invitrogen). Samples were dissociated and homogenized individually using MagNA lyser homogenizer (Roche, France) and serial dilutions of homogenates were plated on GCB plates incubated overnight at 37°C and in a moist atmosphere containing 5% CO2. Bacterial counts were expressed in CFU per implant or murine sample.

Immunohistochemistry and immunofluorescence

In vitro and non-infected engineered constructs

Samples prepared *in vitro* were fixed with 4% paraformaldehyde for 30 min and permeabilized with 0.5% Triton-X-100. They were then directly incubated with primary antibodies directed against CD31 coupled to Alexa Fluor 647 (1/100) at 4°C overnight. Samples were washed with PBS containing 0.1% Triton-X-100 before nuclei staining with 4 ′ ,6-diamidino-2- phenylindole (DAPI) (1/10,000). They were stored in PBS containing 0.02% sodium-azide until image acquisition using 2-photon microscopy.

Twenty-one days after implantation, mice were anesthetized with 3% isofluorane and injected with 50 μl of DyLight 649-labelled Griffonia Simplicifolia isolectin B4 at 1mg/ml and of rhodamine-labelled Ulex Europaeus Agglutinin I at (2mg/ml) into the retro-orbital sinus using a 27-gauge needle. Lectins were allowed to circulate for 15 minutes before sacrifice and harvest of the samples. Tissue constructs were immediately fixed in 4% paraformaldehyde. After overnight incubation they were rinsed and stored in PBS containing 0.02% sodium-azide before processing. Constructs were permeabilized with 2% Triton-X-100 for 5 hours under gentle agitation and immersed in RapiClear 1.52 clearing medium for 3 hours before mounting in the clearing solution with imaging spacers (SunJin Lab) and sealing.

Two-photon imaging was performed on the whole construct (including 3D-printed scaffold) using a Chameleon Discovery laser (Coherent) tuned at 820 nm coupled with a SP8 DIVE microscope (Leica Microsystems, Wetzlar, Germany). Signal was collected through a 25X 0.95NA water immersion objective and detected with non-descanned spectral hybrid and PMT detectors. Z-stacks were acquired with a 3 μm z-step.

Infected engineered constructs

Twenty-one to 49 days after *in vivo* implantation, engineered human microvasculature constructs were surgically removed and fixed with 4% paraformaldehyde for 20 min, then washed with PBS and stored in PBS at 4°C.

For light-sheet microscopy

whole constructs (including 3D-printed scaffold) were permeabilized with 0.5% Triton-X-100 in PBS for 20 min and saturated with 0.5% Triton-X-100 0.1% BSA in PBS during 1 h. The protocol for antibody staining and tissue cleaning was optimized for the incubation time. Samples were incubated for 7 days at 4°C in 0.5% Triton-X-100 in PBS with primary antibodies directed against human CD31 (1/100) coupled to Alexa Fluor 647 (1/100), and anti-*N. meningitidis* coupled to Pacific Blue (1/50). Samples were rinsed and then cleared using RapiClear 1.47, before observation with Zeiss Light-sheet Z1 microscope with 20x detection objective (LSFM clearing 20x/1.0 Corr4915000104) and 10X illumination objective (LSFM clearing 10X/0.2). Light-sheet chamber was filled with 80% TDE/PBS (refractive index of 1.47).

For fluorescence microscopy and Haematoxylin and Eosin (H&E) stain

3D printed supports were removed from the scaffold using scalpel and forceps. The remaining microvasculature without support was frozen in OCT (Tissuetek, Sartorius) and sliced at 10 μm. For histology, microvasculature was stained with H&E. For fluorescence microscopy, samples were permeabilized 5 min with 0.1% Triton-X-100 and then saturated for 15 min using 1% BSA solution. They were then incubated for 2 hours with primary antibodies directed against anti-*N. meningitidis* (1/1000), human CD41 (1/100). They were then incubated for 1 hour with secondary antibodies targeting mouse IgG coupled to Cy5, rabbit IgG coupled to Alexa Fluor 546 or rat IgG coupled to Cy3 (1/200). Nuclei were revealed using DAPI (1/10,000, Invitrogen). Analysis was performed with a Zeiss Observer Apotome 2 using Plan-Apochromat 63x/1.4 oil-immersion objective lens.

QUANTIFICATION AND STATISTICAL ANALYSIS

Information about number of animals used, test used, and measurement of center and dispersion are included in figure legends. Statistical analyses were performed with GraphPad Prism 8.02. Considering the low number of replicates, normality of the distribution of whole data sets were assessed using QQ plot. When needed the data were log transformed. The homogeneity of variance was tested with the Brown-Forsythe F test. In our data, the distribution of the data for each data set respected the normality law and the variance of the groups were homogeneous. Therefore, multiple comparison analyses were assessed with a one-way ANOVA with Bonferroni's multiple comparisons test and data were expressed as geometric mean $\pm$ geometric SD (relevant *p* values were reported in the figures). The H0 hypothesis was rejected for a significance level of $p \leq 0.05$. Statistical analysis reports and descriptive statistics are available in Table S1.